A Super-resolution-based Approach for the Detection of Covid–19 Infection From Chest X-ray Images*

Seema S. Bhat and Hanumantharaju M. C

X-ray is the most accessible imaging modality for detecting Covid-19 infection. However, X-ray image resolution depends on the amount of radiation dose. The Lesser the dosage, the lower the resolution, the higher the noise and patient safety. Detecting Covid-19 infection would be more precise with high-resolution chest X-ray images. The current article explores an edge-preserving single-scale residual learning-based super-resolution method to enhance low-resolution chest X-ray images. We used unsharp masking to preserve small, medium, and high-scale details while super-resolving the given image. The method produces a clear view of the pulmonary opacities in chest X-ray images after super-resolution reconstruction. Statistical feature metrics of first and second-order showed superior quality reconstruction by the proposed method for the given Covid-19 chest X-ray images. Further, to measure the effectiveness of super-resolution, we used an Inception v3 based deep learning model to classify chest X-ray images of Covid-19, pneumonia, and normal class. The performance of the classification model with super-resolved chest X-ray images was tested against 400 images belonging to two different classes at a time. We obtained increased precision of 94% and 96% accuracy in detecting Covid-19 infection in chest X-ray images after super-resolution compared to 64% precision and 68% accuracy before super-resolution.

Seema S. Bhat is currently working as an Assistant Professor in Dept. of Information Scienece and Engineering in Dayananda Sagar College of Engineering, Bengaluru. Her research interests include magnetic resonance imaging and medical image processing.

Hanumantharaju M. C is currently working as a Professor in Dept. of Electronics and Communication in BMS Institute of Technology and Management, Bengaluru. His research interests include VLSI, algorithm design, reconfigurable IC design and image processing.

*Vol.28, No.1, DOI: https://doi.org/10.1007/s12045-023-1530-7

Introduction

Covid-19 is a disease caused by a new strain of severe acute respiratory syndrome coronavirus [1]. The use of reverse-transcriptase polymerase chain reaction (RT-PCR) and nucleic acid amplification tests (NAATs) along with the biomarkers are primarily used for Covid-19 detection and diagnosis [2]. However, the use of RT-PCR and biomarkers take longer and depend on the specimen taken, which could have faults. Imaging provides a faster solution, and the common imaging modalities used for Covid-19 diagnosis are chest computed tomography (CT), chest X-ray (CXR), and lung ultrasonography (LUS) [2]. We can also use magnetic resonance imaging (MRI) and positron-emitting tomography (PET) for pulmonary imaging [3]. Both cannot be used as first-line modalities due to longer scan times and higher costs. Also, PET scanning has a radiation burden. Likewise, LUS diagnosis accuracy depends on the operator's expertise and witnesses low specificity and sensitivity [4]. CT scans have been used frequently in Covid-19 screening, as they provide high anatomic resolution. But, CT scans propagate the menace of contamination and radiation exposure. However, chest X-ray prevents cross-infection among the staff and the patients. X-ray is cost-effective and accessible worldwide [2, 4].

CT scans have been used frequently in Covid-19 screening, as they provide high anatomic resolution. But, CT scans propagate the menace of contamination and radiation exposure.

Chest X-rays can be used from the onset of infection till it turns negative. The severity of lung abnormalities is found to peak at 5–10 days of symptom onset. The mean time from initial positive findings to negative chest X-ray is found to be 10 days(range 6–14 days). Radiologists visualize ground glass patterns, dense opacities obscuring vessels, and bronchial walls in the lungs in Covid-19 chest X-rays [5]. The opacities can damage both lungs at an early stage of Covid-19. Bilateral lower zone consolidation is also a symptom of Covid-19, usually appearing 10–12 days after the disease onset. One of the Covid-19 studies found these symptoms [6], and the study has claimed 69% sensitivity in finding Covid-19 symptoms with baseline chest X-ray images. In recent years, various machine learning models have been applied to solve different tasks, which otherwise was not possible.

In addition, multiple techniques have used deep learning for the enhancement, feature detection, segmentation, and detection of Covid-19 lung lesions [7, 8]. Artificial intelligence based Covid-19 infection detection offers an automated approach to disease diagnosis, thereby reducing reliance on the human eye. The features learned in deep architecture would detect invisible traces of infection, which could not be traced otherwise by the human eyes. These automated methods can be adapted in Covid-19 diagnosis centers as they are inexpensive, quicker, and simpler [9].

X-ray images have low resolution (LR) and possess noise due to low X-ray dosage. Low X-ray dosage is used to maintain patient safety [10]. Pulmonary diseases often have hazy structures. One can obtain more acceptable X-ray images with a higher radiation dose or an expensive imaging setup. Super-resolution is a class of techniques that enhance noisy LR images using a set of high-resolution (HR) images [10, 11]. Super resolution-based enhancement would be easier to get high-quality chest X-rays with minimal radiation dosage to the patients [10]. High-resolution X-ray images may increase the sensitivity and specificity of pathology detection and diagnosis.

X-ray images have low resolution (LR) and possess noise due to low X-ray dosage. Low X-ray dosage is used to maintain patient safety.

Most super-resolution methods are experimented with natural images and eventually extended their proficiencies in medical images. Textures in medical images are more complicated, affluent, and highly correlated [12, 13]. The medical image quality depends on imaging equipment, patient position, and the complicated and unpredictable shape of the scanned organs. Several methods have been proposed based on this aspect [14–16].

According to the literature, single-image super-resolution methods are categorized into three types. The first type is the interpolation method. High computational speed makes interpolation-based methods suitable for parallel computing [17, 18]. They do not produce valuable high-frequency details [18]. Therefore, it is hard to obtain sharp and high-resolution images with interpolation-based methods [18].

Super-resolution reconstruction (SRR) uses the HR reference im-

age to improve the resolution of the LR image [19–23]. Reconstruction-based methods are typically dependent on well-designed priors. Most of them do not capture the complete characteristics of image priors, as they use shallow features of the image and manually chosen parameters [11, 14, 24]. Nevertheless, the hand-crafted tuning parameters make operations more complicated and prone to errors. However, without much information on image priors and repetitive patterns, these methods yield objectionable edges [11, 14].

Super-resolution reconstruction (SRR) uses the high-resolution reference image to improve the low-resolution image.

In the third type, super-resolution images produce the corresponding HR version by learning the mapping function between LR and HR images [25–28]. Dictionary-based super-resolution methods consume more time to build dictionaries and reconstruct HR versions with limited real-time medical data. Also, optimizing the performance in every stage of learning and reconstructing is a tedious job.

Deep learning-based super-resolution methods extract image features implicitly to get high-resolution images.

Deep learning-based super-resolution methods extract image features implicitly to get HR images. Mapping is done automatically through convolution operations to enhance details. The first convolutional neural network (CNN) for super-resolution had three layers [29]. However, the deep learning literature has various deep network architectures for super-resolution [15, 29–34]. Deep architectures allow SR methods to expand their receptive field and capture more contextual details over large image regions. With the same weight parameters for all the convolutional layers, a deeply recursive SR technique in [30] did not change the receptive field size. Tai et al. stacked numerous residual recursive blocks to get a better model [32]. Kang et al. used ResNet architecture with wavelets to denoise and preserve texture in low-dose CT/ X-ray images [33]. Frequency localization properties of the wavelets preserve small-scale structures in the given low-dose X-ray images. Residual learning bypassed the low-frequency wavelet coefficients and, added with the denoised wavelet coefficients, made training more efficient. The larger receptive field enhanced the performance of the proposed method. However, the larger receptive field results in a deeper network.

Also, input images of lower thickness lost high-frequency details and produced blurred edges after reconstruction [33]. Xu et al. proposed GAN-based super-resolution for chest X-ray images with auxiliary label information for feature extraction and spectral normalization for good performance [15]. However, GAN-based SR methods are known to add noise while enhancing high-frequency details. Also, a few details were lost during the partial enlargement of regions of interest [15].

Taking more image contexts into account would miss high-frequency components in super-resolution [10, 11]. Expanding the receptive field deepens the architecture and enlarges the filter size [34]. This expansion also results in multiple parameters to tune while training and reduces the performance of the model [34]. Moreover, any medical imaging needs additional prior details compared to natural images. It is also complicated to enhance intricate structures and preserve sensitive details. Additionally, medical images have a relatively small dataset. It is not easy to collect clinical high- and low-resolution image pairs. The current work adapts the ResNet-based super-resolution network architecture proposed by Lim et al. [31]. In the second phase, we detect Covid-19 infection in the given chest X-ray image using an Inception v3-based classification model trained by super-resolved chest X-ray images. We use a residual learning-based convolution neural network (CNN) with unsharp masking to obtain SR Covid-19 chest X-ray images in this work. *Figure* 1 shows the single-scale residual network architecture used in the current work. All experiments were conducted with a GPU graphics card on Google Colaboratory with Windows 10 OS.

It is not easy to collect clinical high- and low-resolution image pairs.

The major highlights of this work are listed below:

1. We present a deep learning-based super-resolution method for Covid-19 chest X-ray images. High-resolution chest X-ray images would assist in the precise diagnosis of the disease.

2. We used a single-scale residual network model to reduce noise and amplify details in the low-resolution chest X-ray images. The residual network reduces noise and is followed by unsharp

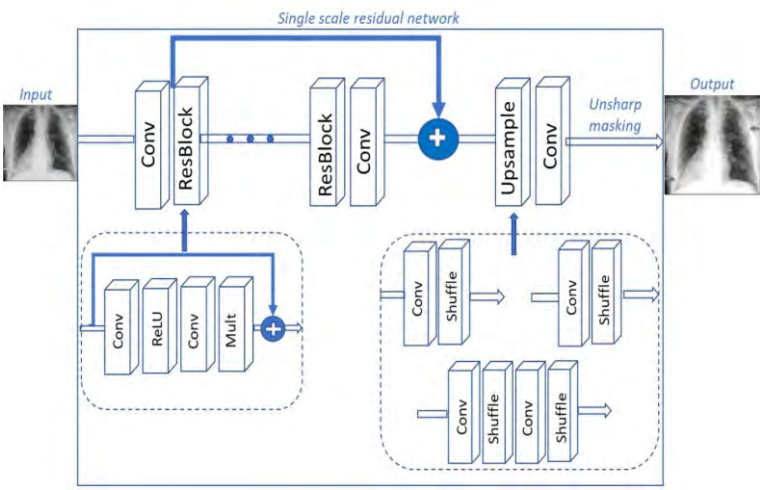

Figure 1. Workflow of the proposed method. We use edge-preserving single-scale residual network for Covid-19 chest X-ray super resolution.The network architecture is adpated from [31]. Unsharp masking is used to preserve details in the test samples.

masking, which is an edge-preserving high-pass filter that safeguards intricate details in chest X-ray images.

3. To improve the accuracy of Covid-19 chest X-ray image enhancement and quantitative assessment, we use the geometric self-ensemble strategy.

4. We could detect Covid-19 infection in a given chest X-ray image with more than 96% accuracy after super-resolution.

Materials and Methods

The proposed method works in two phases. In the first phase, we propose an edge-preserving super-resolution deep learning model to enhance low-resolution chest X-ray images. In the second phase, we detect Covid-19 infection in the given chest X-ray image using a classification model.

Phase 1: Edge-preserving Super-resolution Deep Learning Model

Dataset: The experiment uses the DIV2K dataset for training [35]. DIV2K has 800 training images, 100 validation images, and 100 test images of high quality with 2K resolution. The testing phase used selected samples from the COVID-19 chest X-

ray public dataset [36]. The dataset exclusively has 123 frontal view chest X-ray images. There are 244 total samples, including Covid-19 and other viral/ bacterial pneumonia in the posterior-anterior (PA) or vice-versa (AP) view of chest CT and X-ray images. It also has 38 samples of AP supine[1] view chest images. Though public Covid-19 chest X-ray images are available, they include non-Covid-19, pneumonia, and other chest X-ray images. There is no gold standard HR chest X-ray images specified in the test set. So, we reported and compared the performances on the DIV2K validation dataset.

[1] Supine anteroposterior view.

Network archirecture: *Figure* 1 shows the network architecture used to super-resolve the Covid-19 chest X-ray images. Each residual block in an edge-preserving single-scale residual network has two convolution layers. The first convolutional layer does feature extraction, and the last convolution layer does the nonlinear mapping. Eliminating batch normalization and final ReLU layers from the residual block in a single-scale residual network increases the super-resolution performance.

Each residual block in an edge-preserving single-scale residual network has two convolution layers.

Training and testing: The proposed super-resolution model uses 800 DIV2K training images. The model uses image patches of size 48×48 and normalized before training. Augmentation of the image patches includes 90° rotations and random horizontal flips. The training uses 30,000 steps with a constant learning rate of 1×10^{-4} and utilizes l_1 loss instead of l_2 for better convergence.

Testing was done on selected samples of matrix size—365×435—from the Covid-19 chest X-ray public dataset by Cohen [36]. Linear unsharp masking increases small-scale acutance to emphasize the texture and details of the given image [37]. Unsharp masking is an edge-preserving high-pass filter used in the testing phase of the proposed method to sharpen the edges of the reconstructed images [38]. The radius in unsharp masking decides the size of the edge to be enhanced. A larger radius affects small edges and vice versa. The magnitude and sharpness of the sharpened image depend on the amount[2] and threshold. A radius = 4, amount = 1 and threshold/scaling factor = 0.5 made reconstructed images sharper.

[2] The amount represents how intense the user wants the sharpening to be. A low amount setting results in rather mild sharpening lines, but a high amount setting produces extremely dark and extremely light lines.

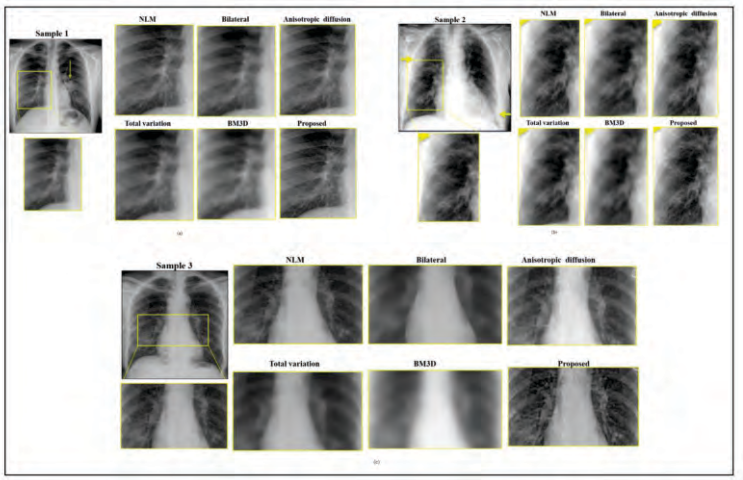

Figure 2. Visual represenation of the proposed super-resolution and edge preserving comparative methods of COVID-19 chest X-ray images.The figure shows visual quality of the edge-preserving single scale residual-based super resolution method and state of the art edge-preserving algorithms on chosen three samples.Loss of contour and other details are observed in the case of bilateral, total variation and BM3D reconstructed COVID-19 chest X-ray images.NLM and anisotropic diffusion witnessed loss of small and medium contrast details. The proposed method was able to preserve and enhance the details.

The final up-sampling layer includes a convolutional layer followed by a shuffle for ×2, ×3, and ×4 upscaling factors. Each convolutional layer produces sixty-four feature maps. The depth of the network and the number of feature channels used are 32 and 256, respectively. The experiment used a scaling factor of 0.1.

The self-ensemble strategy is similar to [31] used in the testing phase. Input image I^{LR} to generate seven augmented inputs: $I^{LR}_{n,i} = T_i(I^{LR}_{n,i})$, where T_i represents transformation function, including identity by flipping and rotating. For every augmented image, the proposed model generated a corresponding super-resolved image $I^{SR}_{n,i}$ with $i = 1$ to 8. Later, the inverse transform is applied to get the original geometry. Final SR images are obtained by averaging the inverse transform $I^{SR}_{n,i} = \frac{1}{8}\sum_1^8 T_i^{-1} I^{SR}_{n,i}$.

The performance evaluation of the proposed method included a comparison with the state-of-the-art edge-preserving algorithms: BM3D, anisotropic diffusion total variation, bilateral filters, and nonlocal means.

Performance evaluation and comparative methods: The performance evaluation of the proposed method included a comparison with the state-of-the-art edge-preserving algorithms: BM3D, anisotropic diffusion total variation, bilateral filters, and nonlocal means [39–41]. These are edge-preserving filters, initially designed for realistic images, but extend their applications successfully to X-ray image enhancement and other medical imaging modalities [38–41]. The implementation of these algorithms

is officially available on the internet. All of these algorithms use the same set of normalized images from the test dataset for execution.

All the above-mentioned edge-preserving algorithms have at least one controlling parameter. We have used either maximum value or default values for the tuning parameters of these state-of-the-art edge-preserving algorithms. BM3D algorithms eliminate correlated stationary noise in the given image. It uses two tuning parameters for noise reduction: σ and hard threshold to map the pixel values. We have used the variance of the given image for parameter σ and default hard thresholding for image reconstruction.

Anisotropic diffusion algorithms require the number of iterations, conduction coefficient κ, stability parameter γ, and choosing an option between Perona–Malik diffusion equation 1 or 2. The current work uses iterations = 50, $\kappa = 50$, $\gamma = 0.2$, and equation 2 to reconstruct X-ray images. Total variation measures the similarity and dissimilarity of pixels to find the meaningful relationship between them. The smoothing parameters use a weight of 0.1 in the total variation experiment with Covid-19 chest X-ray images.

Anisotropic diffusion algorithms require the number of iterations, conduction coefficient κ, stability parameter γ, and choosing an option between Perona–Malik diffusion equation 1 or 2.

A bilateral filter needs the diameter of the pixel neighborhood and parameter σ for color and coordinate space. For larger values of color and coordinate σ values, greater will be the mixing of pixels in the given range. We have used diameter = 15, σ color, and coordinate space = 75 each in the present work.

NLM method uses luminance component regulator h, template window size. The weight of the template patch is computed in terms of pixels and search window size. The window size is used to compute the weighted average for a given pixel. The default values 3, 7, and 21 are used correspondingly for the NLM, as mentioned earlier.

In this work, *ImageJ*, a platform-independent image processing tool, was used for plotting edges in LR and HR chest X-ray images. We obtained sharper edges after super-resolution reconstruction. Finding edges in LR and SR X-ray images indicates

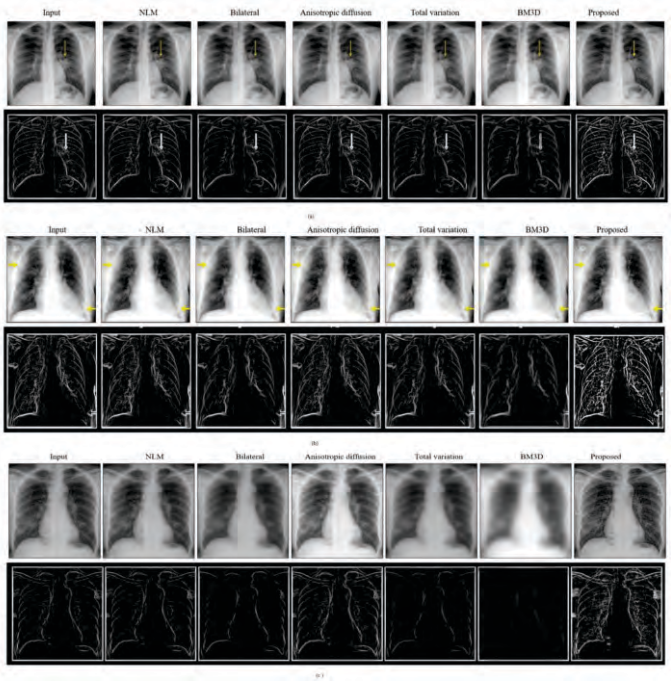

Figure 3. Visual representation of edge-preservation of the proposed and comparative methods. The comparison of small-, medium-, and high-scale edges of the proposed edge-preserving super-resolution method with the state-of-the-art algorithms for the chosen three samples is shown. Enhanced edges produced by the proposed super-resolution method can be observed for the chosen sample in the last column.

detail preservation by SR reconstruction. *Find Edges* application of *ImageJ* facilitated visualization of edge-preservation with comparative and proposed methods [42].

Evaluation metrics: We evaluated the proposed and comparative edge-preserving algorithms' performance with texture-related metrics. We do not use measures like PSNR, or SSIM, which are correlated with human perception, for two reasons. The first reason is that while performing this study, there were no gold standard reference Covid-19 chest X-ray images, and the second reason is that texture has more importance in medical diagnosis. A clear texture simplifies clinical diagnostics [15] [43–45]. We used selected blind reference metrics derived from first and second-order statistical feature measures. First-order statistical feature metrics are mean, standard deviation, and entropy. They are used to measure the contrast and brightness of reconstructed images. Entropy measures the content of the image; the higher the entropy richer the details in the given image.

Second-order statistical metrics—contrast, homogeneity, energy,

and correlation are obtained using the grey-level co-occurrence matrix (GCLM). They play a significant role in the measure of image sharpness [45]. The larger the changes in grey levels, the higher contrast and sharpness. GCLM energy defines the overall probability of unique gray-scale patterns in the image. To summarize, higher mean, standard deviation, entropy, contrast, and correlation indicate the reconstructed image's superior quality, whereas energy and homogeneity decrease with image quality.

Second-order statistical metrics—homogeneity, energy, and correlation are obtained using the grey-level co-occurrence matrix. They play a significant role in the measure of image sharpness.

Phase 2: Classification Model for Covid-19 Infection Detection

We evaluated the effectiveness of the super-resolution method for the given chest X-ray images before and after super-resolution using a classification model. We utilized VGG16 and Inception v3 models as base models. We used normal, Covid-19, and pneumonia chest X-ray images from the COVID-19 Radiography Database by Kaggle. It had 3616 Covid-19 positive cases along with 10,192 normal and 1345 pneumonia chest X-ray images. The classification model labelled the given chest X-ray image under covid and non-covid (normal and pneumonia) class.

Training and testing: In the first phase, the training and testing experiments included Covid-19 and normal chest X-ray image pairs from the Kaggle database. The model was trained on 200 samples of each Covid-19 and normal images before and after super-resolution. All the images used for training were augmented, normalized, and resized to 224×224 dimension. The batch size (BS) was set to 16, and a learning rate of 1e-4 was used throughout the training. The training labeled each chest X-ray image to covid or non-covid class based on classification probability. We plotted a receiver operating characteristic (ROC) curve to visualize the performance of the classification. Also, a confusion matrix was created to compare the actual target chest X-ray images with the images predicted by the classification model. We computed the precession, F1-score, recall, and accuracy of the classification model for both covid and non-covid classes. We measured the testing loss and testing accuracy of the classification model. In the second phase, training and testing were repeated for

Covid-19 and pneumonia chest X-ray image pairs before and after super-resolution. In total, we tested 800 chest X-ray images belonging to Covid-19 and normal and Covid-19 and pneumonia classes. Test loss and test accuracy were computed before and after super-resolution.

Performance evaluation: To evaluate the performance of the classification model, we used four common measures. They are—precision, recall, accuracy, and F1 score—as described as below [46]:

$$Precision = \frac{TP}{(TP + FP)}. \tag{1}$$

$$Recall = \frac{TP}{(TP + FN)}. \tag{2}$$

$$F1\ score = 2 * \frac{(Precision * Recall)}{(Precision + Recall)}. \tag{3}$$

$$Accuracy = \frac{(TN + TP)}{(TN + TP + FN + FP)}. \tag{4}$$

Here, TP is the count of true positive samples, TN is the count of true negative samples, FP is the count of false positive samples, and FN is the count of false negative samples from a confusion matrix.

Results and Discussion

The experiment involved three randomly chosen samples from the test set. The first column in *Figure* 2 shows the test images chosen with a posterior-anterior (PA) view of the patient. The rest of the columns in *Figure* 2 show reconstructed images of chosen edge-preserving filters and the proposed method. We enlarged randomly chosen regions to view the lung bronchioles, alveolus, and ground-glass opacities in the reconstructed images.

Edge-preserving algorithms are supposed to retain details while removing the noise from the given image.

Edge-preserving algorithms are supposed to retain details while removing the noise from the given image. For the given sample, there wasn't much difference in the details observed in the NLM and anisotropic diffusion (AD) filter in the magnified regions. Noise present in small-scale features of X-ray images foils accurate averaging of coefficients and generates artifacts in NLM filters. In the anisotropic diffusion method, the regularization parameter's optimal value depends on the prior knowledge of the noise. AD smoothens flat regions, and the tuning regularization parameter is complex. However, noise reduction resulted in blurred edges in the bilateral, total variation, and BM3D filters. It is hard to observe the contour and other details in their reconstructed counterpart. The reason is, in high gradient regions, bilateral filters tend to produce cartoonish texture. At the same time, the performance of BM3D worsens with higher levels of noise in the images. The total variation filters tend to lose contrast during image restoration; hence blurring small- and medium-scale edges are observed.

The reconstructed results from the proposed method, edges, and other details were well preserved, as shown in *Figure* 2(a–c). The larger receptive fields can capture small- and medium-scale edges in X-ray images, and residual learning can propagate these features to the deepest layers. Also, the proposed method learns features implicitly; it does not require prior knowledge of the noise distribution. Single-scale residual blocks can effectively eliminate noise. Unsharp masking is a postprocessing technique that preserves high-frequency details in the reconstructed image.

We generated the edge maps to visualize the amount of edge preservation of each technique mentioned earlier. *Figure* 3(a–c) shows edge maps of the proposed and comparative edge-preserving filters. NLM and anisotropic filters were able to retain most of the edges like in the given three samples. However, bilateral, total variation, and BM3D reconstructed images suffered from loss of low-frequency edges. Unsharp masking is a powerful way of enhancing edges in the given images. In the proposed method, unsharp masking helped to retain low-scale and high-scale details

(see last column in *Figure* 3 (a–c)).

We evaluated the proposed and comparative methods using statistical feature measures of first and second orders because the standard reference image was unavailable. The first-order metrics include individual pixels to evaluate the performance. The mean and standard deviation of the reconstructed images show pixel intensities in the given image. The proposed method obtained a higher mean and standard deviation than its LR counterpart and some comparative filters. Entropy indicates information present in the given image. The proposed method's higher entropy values for all three samples indicate high-intensity levels and high contrast in reconstructed images. The plots in *Figure* 4 summarizes first-order statistical measures for the given samples and their reconstructed images. The proposed method exhibits the best entropy and standard deviation values compared to other edge-preserving algorithms. Total variation and BM3D obtained pretty good values. However, the mean, standard deviation, and entropy values obtained using NLM, bilateral, and anisotropic diffusion algorithms were similar to those of the input samples.

The second-order statistical measures incorporate the neighborhood of pixels to evaluate the performance of the image processing techniques and impact the sharpness of the given image. We obtained the second-order statistics by constructing a GLCM matrix for each of the above-mentioned edge-preserving methods. GCLM details the positions of the pixels with similar gray levels in the image. It is obvious to notice higher contrast and correlation values for the proposed method in *Figure* 5. Also, the proposed method obtained lower energy and homogeneity values. Lower energy and homogeneity values indicate a lower localized change in the image. We obtained higher contrast and correlation values for the proposed method, indicating superior sharpness and brightness.

We evaluated the performance of the proposed super-resolution using a classification model. *Figure* 4 shows the sample images belonging to Covid or non-Covid classes. *Figure* 5 shows selected

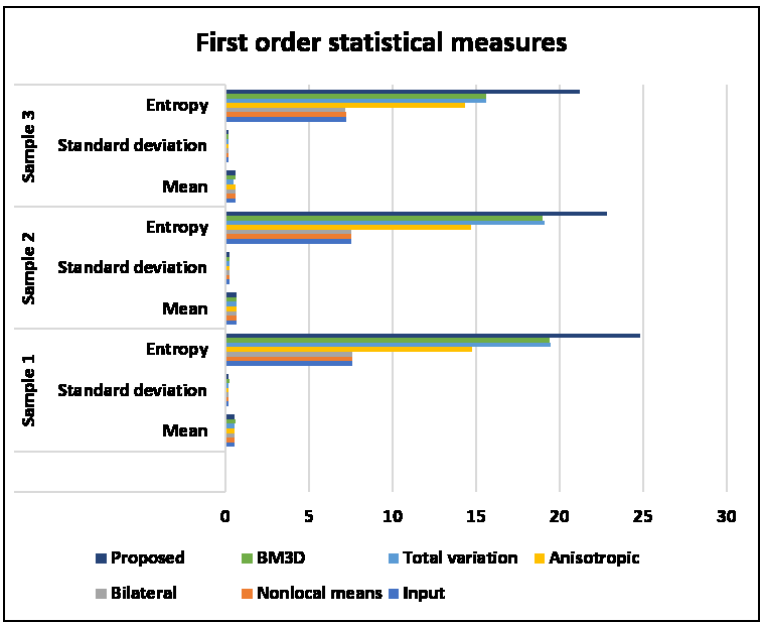

Figure 4. Image reconstruction results using first-order statistical metrics. We computed the mean, standard deviation, and entropy of the proposed edge-preserving super-resolution method with state-of-the-art edge-preserving algorithms. The proposed method obtained a higher mean and entropy than the other methods.

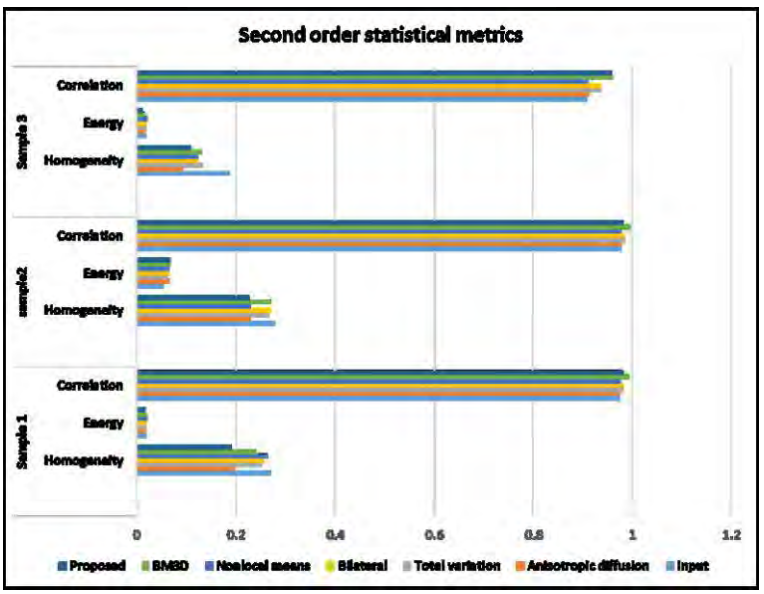

Figure 5. Performance evaluation using second-order statistical metrics. We computed homogeneity, energy, and correlation of the proposed edge-preserving super-resolution method with state-of-the-art edge-preserving algorithms. The proposed method's good quantitative values ensured enhanced contrast and brightness after super-resolution.

images obtained after model prediction whether the test image is Covid or non-Covid with its probability. The model classifies the

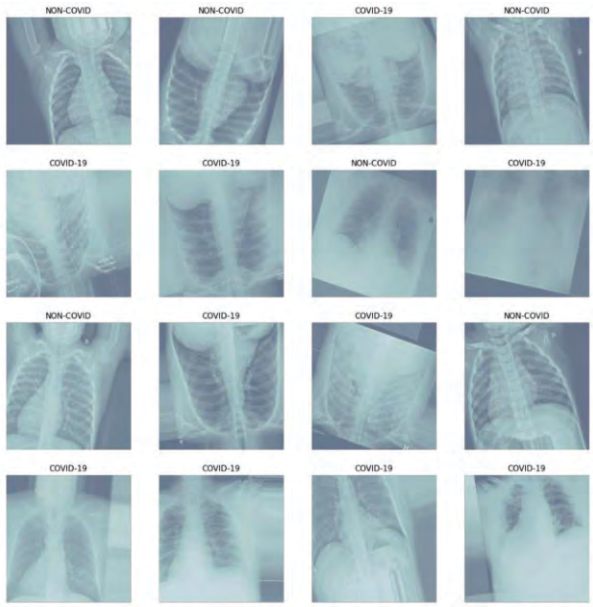

Figure 6. Sample images from training and testing with their class labels. The labels are assigned by the classification model by extracting features from each image during the training phase.

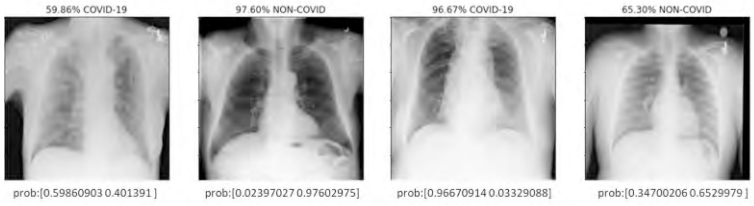

Figure 7. Test image prediction samples with their probability value. A probability higher than 0.5 is considered to be the Covid class. The probabilities are calculated during the training of the classification network.

test images as covid if the probability is more than 0.5. Otherwise, the model classifies the test image as non-Covid.

We computed the test loss and test accuracy before and after super-resolution for 800 chest X-ray images belonging to Covid-19 and normal and Covid-19 and pneumonia classes. We obtained a test loss of 0.7160 and a test accuracy of 0.6399 before super-resolution. Higher test accuracy of 0.7599 and lower test loss of 0.3759 were attained after super-resolution.

Figure 6 shows ROC curves obtained for classifying Covid-19 and normal chest X-ray images. The curve is closer to the upper

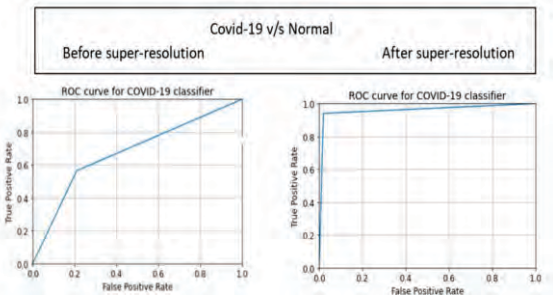

Figure 8. ROC curve for Covid-19 versus normal chest X-ray images. The curve closer to the upper left corner indicates higher test accuracy. The curve closer to the corner after super-resolution indicates higher classification accuracy.

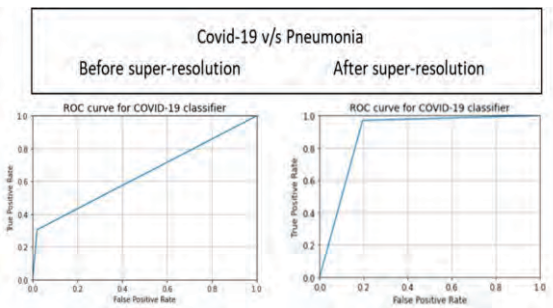

Figure 9. ROC curve for Covid-19 versus pneumonia chest X-ray images. The curve closer to the corner after super-resolution shows higher classification accuracy in predicting Covid and non-Covid images.

left corner, which indicates higher test accuracy. It is evident that ROC curve obtained after super-resolution has increased sensitivity in detecting Covid-19. *Figure* 7 shows ROC curves plotted for Covid-19 and pneumonia image classification. Obviously, a better ROC curve is noticed after super-resolution. *Figure* 8 and 9 show confusion matrix Covid and non-Covid class images. The proposed method labeled 196 Covid-19 images out of 200 images after super-resolution compared to before super-resolution values 127 and 158.

Table 1 and 2 shows precision, recall, and F1 score values before and after super-resolution. We obtained higher precision and recall values after super-resolution. The classification accuracy increased from 0.68 to 0.96 after super-resolution in Covid-19 and normal class. At the same time, we obtained an increase in accuracy for Covid-19 and pneumonia cases.

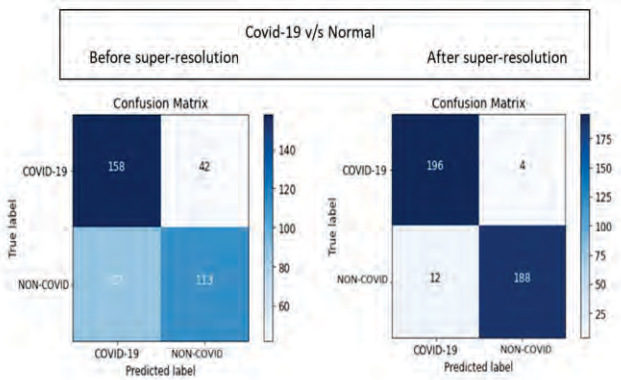

Figure 10. Confusion matrix Covid-19 versus normal chest X-ray images. An increase in classification accuracy after super-resolution can be observed.

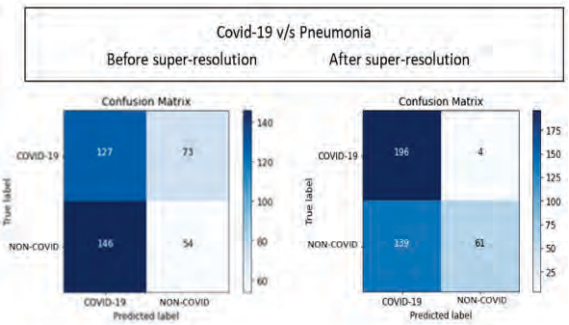

Figure 11. Confusion matrix Covid-19 versus pneumonia chest X-ray images. An increase in classification accuracy after super-resolution can be observed.

Conclusion

The proposed deep learning-based edge-preserving super-resolution method is used to obtain high-resolution Covid-19 chest X-ray images to detect Covid-19 infection. Unsharp masking during the testing phase preserves details, and a single-scale residual network reduces inherent noise in Covid-19 chest X-ray images. The

Table 1. Precision, recall, F1 score, and accuracy of classification model before and after super-resolution for Covid-19 versus normal class. Improved values in all the classification metrics can be observed after super-resolution.

		2 way: Covid v/s Normal			
		Precision	Recall	F1 score	Accuracy
Before super-resolution	Covid-19	0.64	0.79	0.71	0.68
	Normal	0.73	0.56	0.64	
After super-resolution	Covid-19	0.94	0.98	0.96	0.96
	Normal	0.98	0.94	0.96	

		2 way: Covid v/s Pneumonia			
		Precision	Recall	F1 score	Accuracy
Before super-resolution	Covid-19	0.47	0.64	0.54	0.45
	Pneumonia	0.43	0.27	0.33	
After super-resolution	Covid-19	0.59	0.98	0.73	0.64
	Pneumonia	0.94	0.30	0.46	

Table 2. Precision, recall, F1 score, and accuracy of classification model before and after super-resolution for Covid-19 versus pneumonia class. We obtained higher classification metrics as expected after super-resolution.

experimental results show that the proposed method can effectively reconstruct Covid-19 features compared to other state-of-the-art techniques. Higher entropy, contrast values, and lower homogeneity energy values in performance evaluation ensured superior quality reconstruction of the proposed method. The classification model trained using super-resolved chest X-ray images obtained higher accuracy of 96%. However, analysis has been done on limited data, and only preliminary results have been obtained. The enhancement schemes are purely exploratory and do not include clinical trials/medical validations of the approach. Also, there is a potential risk of generating features not part of the target images. Network optimization and effective mapping between low- and high-resolution feature space can be potential future work.

Suggested Reading

[1] **Na Zhu et al., A novel coronavirus from patients with pneumonia in China, 2019. *New England Journal of Medicine*, 20;382(8), pp.727–733, 2020.**

[2] **Tinotenda A Harahwa et al., The optimal diagnostic methods for Covid-19. *Diagnosis*, Vol.7, No.4, pp.349–356, 2020.**

[3] **Brandon K K Fields, Natalie L Demirjian, Habibollah Dadgar and Ali Gholamrezanezhad, Imaging of Covid-19: CT, MRI, and PET, In *Seminars in Nuclear Medicine*, Vol.51, pp.312–320. Elsevier, 2021.**

[4] **Liqa A Rousan, Eyhab Elobeid, Musaab Karrar and Yousef Khader, Chest X-ray findings and temporal lung changes in patients with Covid-19 pneumonia, *BMC Pulmonary Medicine*, Vol.20, No.1, pp.1–9, 2020.**

[5] **V N Manjunath Aradhya, Mufti Mahmud, D S Guru, Basant Agarwal, and M Shamim Kaiser, One shot cluster based approach for the detection of Covid-19 from chest X-ray images, *Cogn Comput.*, 13(4), pp.873–881, 2021.**

[6] **Ho Yuen Frank Wong et al., Frequency and distribution of chest radiographic findings in patients positive for Covid-19, *Radiology*, Vol.296, No.2, pp.E72–E78, 2020.**

[7] Seema S Bhat, M C Hanumantharaju, and V N Manjunath Aradhya, Super resolution techniques for Covid-19 chest X-ray images, In *Computer Communication, Networking and IoT*, pp.549–558. Springer, 2021.

[8] Sudhen B Desai, Anuj Pareek, and Matthew P Lungren, Deep learning and its role in Covid-19 medical imaging, *Intelligence-based Medicine*, Vol.3, 100013, 2020.

[9] Shashank Vaid, Reza Kalantar and Mohit Bhandari, Deep learning Covid-19 detection bias: Accuracy through artificial intelligence, *International Orthopaedics*, Vol.44, pp.1539–1542, 2020.

[10] Masato Shimizu, Hidetoshi Kariya, Tomio Goto, Satoshi Hirano and Masaru Sakurai, Super-resolution for X-ray images, In *2015 IEEE 4th Global Conference on Consumer Electronics (GCCE)*, pp.246–247, IEEE, 2015.

[11] Yoshiki Sano, Takuma Mori, Tomio Goto, Satoshi Hirano and Koji Funahashi, Super-resolution method and its application to medical image processing, In *2017 IEEE 6th Global Conference on Consumer Electronics (GCCE)*, pp.1–2, IEEE, 2017.

[12] Yang Li, Wei Liang, Haibo An, Yinlong Zhang and Jindong Tan, C-arm based image-guided percutaneous puncture of minimally invasive spine surgery, In *2017–10th International Congress on Image and Signal Processing, BioMedical Engineering and Informatics (CISP-BMEI)*, pp.1–5. IEEE, 2017.

[13] Concetto Spampinato, Simone Palazzo, Daniela Giordano, Marco Aldinucci and Rosalia Leonardi, Deep learning for automated skeletal bone age assessment in X-ray images, *Medical Image Analysis*, Vol.36, pp.41–51, 2017.

[14] Kensuke Umehara, Junko Ota, Naoki Ishimaru, Shunsuke Ohno, Kentaro Okamoto, Takanori Suzuki, and Takayuki Ishida, Performance evaluation of super-resolution methods using deep-learning and sparse-coding for improving the image quality of magnified images in chest radiographs, *Open Journal of Medical Imaging*, Vol.7, No.3, pp.100–111, 2017.

[15] Liming Xu, Xianhua Zeng, Zhiwei Huang, Weisheng Li and He Zhang, Low-dose chest X-ray image super-resolution using generative adversarial nets with spectral normalization, *Biomedical Signal Processing and Control*, Vol.55, p.101600, 2020.

[16] Chenyu You et al., CT super-resolution gan constrained by the identical, residual, and cycle learning ensemble (GAN-circle), *IEEE Transactions On Medical Imaging*, Vol.39, No.1, pp.188–203, 2019.

[17] Michel Bätz, Andrea Eichenseer, Jürgen Seiler, Markus Jonscher and Andre Kaup, Hybrid super-resolution combining example-based single-image and interpolation-based multi-image reconstruction approaches, In *2015 IEEE International Conference On Image Processing (ICIP)*, pp.58–62. IEEE, 2015.

[18] Robert Keys, Cubic convolution interpolation for digital image processing, *IEEE Transactions On Acoustics, Speech, and Signal Processing*, Vol.29, No.6, pp.1153–1160, 1981.

[19] Michal Irani and Shmuel Peleg, Super resolution from image sequences, In *Proceedings 10th International Conference on Pattern Recognition*, Vol.2, pp.115–120. IEEE, 1990.

[20] Zhouchen Lin and Heung-Yeung Shum, Fundamental limits of reconstruction-

based super-resolution algorithms under local translation, *IEEE Transactions On Pattern Analysis and Machine Intelligence*, Vol.26, No.1, pp.83–97, 2004.

[21] Henry Stark and Peyma Oskoui, High-resolution image recovery from image-plane arrays, using convex projections, *JOSA A*, Vol.6, No.11, pp.1715–1726, 1989.

[22] Richard R Schultz and Robert L Stevenson, Extraction of high-resolution frames from video sequences, *IEEE Transactions On Image Processing*, Vol.5, No.6, pp.996–1011, 1996.

[23] Krishna Ratakonda and Narendra Ahuja, POCS based adaptive image magnification, In *Proceedings 1998 International Conference on Image Processing*, ICIP98 (Cat. No. 98CB36269), pp.203–207, IEEE, 1998.

[24] Mufti Mahmud et al., Deep learning in mining biological data, *Cogn. Comput.*, Vol.13, No.1, pp.1–33, January 2021.

[25] Sam T Roweis and Lawrence K Saul, Nonlinear dimensionality reduction by locally linear embedding, *Science*,Vol.290, No.5500, pp.2323–2326, 2000.

[26] Radu Timofte, Vincent De Smet and Luc Van Gool, Anchored neighborhood regression for fast example-based super-resolution, In *Proceedings of the IEEE International Conference on Computer Vision*, pp.1920–1927, 2013.

[27] Junjun Jiang, Xiang Ma, Chen Chen, Tao Lu, Zhongyuan Wang and Jiayi Ma, Single image super-resolution via locally regularized anchored neighborhood regression and nonlocal means, *IEEE Transactions on Multimedia*, Vol.19, No.1, pp.15–26, 2016.

[28] Jianchao Yang, John Wright, Thomas S Huang, and Yi Ma, Image super-resolution via sparse representation, *IEEE Transactions On Image Processing*, Vol.19, No.11, pp.2861–2873, 2010.

[29] Chao Dong, Chen Change Loy, Kaiming He and Xiaoou Tang, Image super-resolution using deep convolutional networks, *IEEE Transactions on Pattern Analysis and Machine Intelligence*, Vol.38, No.2, pp.295–307, 2015.

[30] Jiwon Kim, Jung Kwon Lee, and Kyoung Mu Lee, Deeply-recursive convolutional network for image super-resolution, In *Proceedings of the IEEE Conference on Computer Vision and Pattern Recognition*, pp.1637–1645, 2016.

[31] Bee Lim, Sanghyun Son, Heewon Kim, Seungjun Nah and Kyoung Mu Lee, Enhanced deep residual networks for single image super-resolution, In *Proceedings of the IEEE Conference on Computer Vision and Pattern Recognition Workshops*, pp.136–144, 2017.

[32] Ying Tai, Jian Yang and Xiaoming Liu, Image super-resolution via deep recursive residual network, In *Proceedings of the IEEE Conference on Computer Vision and Pattern Recognition*, pp.3147–3155, 2017.

[33] Eunhee Kang, Won Chang, Jaejun Yoo and Jong Chul Ye, Deep convolutional framelet denosing for low-dose CT via wavelet residual network, *IEEE Transactions on Medical Imaging*, Vol.37, No.6, pp.1358–1369, 2018.

[34] Yulun Zhang, Yapeng Tian, Yu Kong, Bineng Zhong, and Yun Fu, Residual dense network for image super-resolution, In *Proceedings of the IEEE Conference on Computer Vision and Pattern Recognition*, pp.2472–2481, 2018.

[35] Radu Timofte, Shuhang Gu, Jiqing Wu, and Luc Van Gool, NTIRE 2018 challenge on single image super-resolution: Methods and results, In *Proceedings of*

the IEEE Conference on Computer Vision and Pattern Recognition Workshops, pp.852—863, 2018.

[36] J P Cohen, P Morrison, L Dao, K Roth, TQ Duong and M Ghassemi, Covid-19 image data collection: Prospective predictions are the future, *The Journal of Machine Learning for Biomedical Imaging*, 2, pp.1–38, Dec 2020.

[37] Radu Ciprian Bilcu and Markku Vehvilainen, Constrained unsharp masking for image enhancement, In: Elmoataz, A., Lezoray, O., Nouboud, F., Mammass, D. (eds) *Image and Signal Processing*, ICISP 2008. *Lecture Notes in Computer Science*, Vol.5099. Springer, Berlin, Heidelberg. https://doi.org/10.1007/978-3-540-69905-7_2.

[38] Tommaso Cerciello, Paolo Bifulco, Mario Cesarelli and Antonio Fratini, A comparison of denoising methods for x-ray fluoroscopic images, *Biomedical Signal Processing and Control*, Vol.7, No.6, pp.550–559, 2012.

[39] Eric Michel-González, Min Hyoung Cho and Soo Yeol Lee, Geometric nonlinear diffusion filter and its application to X-ray imaging, *Biomedical Engineering Online*, Vol.10, No.1, pp.1–16, 2011.

[40] Dang Thanh et al., A review on CT and X-ray images denoising methods, *Informatica*, Vol.43, No.2, 2019.

[41] Mugahed A Al-Antari, Mohammed A Al-Masni, Mo-hamed K Metwally, Dildar Hussain, Se-Je Park, Jeong-Sik Shin, Seung-Moo Han, and Tae-Seong Kim, Denoising images of dual energy X-ray absorptiometry using non-local means filters, *Journal of X-ray Science and Technology*, Vol.26, No.3, pp.395–412, 2018.

[42] Wayne S Rasband et al., *Imagej*, 1997.

[43] Norman Burningham, Zygmunt Pizlo and Jan P Allebach, Image quality metrics, *Encyclopedia of Imaging Science and Technology*, 2002.

[44] M C Hanumantharaju, V N Manjunath Aradhya and G Hemantha Kumar, Understanding and analysis of enhanced Covid-19 chest X-ray images, In *Intelligent Systems and Methods to Combat Covid-19*, pp.47–55. Springer, 2020

[45] V L Jaya and R Gopikakumari, IEM: A new image enhancement metric for contrast and sharpness measurements, *International Journal of Computer Applications*, Vol.79, No.9, 2013.

[46] Cyril Goutte and Eric Gaussier, A probabilistic interpretation of precision, recall and f-score, with implication for evaluation, In *European Conference on Information Retrieval*, pp.345–359. Springer, 2005.

Address for Correspondence
Seema S. Bhat
#77, Ankura
1st main, 2nd stage
Arakere Micolayout
Bengaluru 560 076, India.
Email:
seemasbhat@dayanandasagar.edu
Hanumantharaju M. C
Email:
mchanumantharaju@bmsit.in